Vibrational dynamics of single-crystal YVO_4 studied by polarized micro-Raman spectroscopy and *ab initio* calculations

Andrea Sanson
Dipartimento di Fisica e Astronomia "G. Galilei", Università degli Studi di Padova, Via Marzolo 8, I-35131 Padova, Italy

Marco Giarola, Barbara Rossi, and Gino Mariotto*
Dipartimento di Informatica, Università degli Studi Verona, Strada Le Grazie 15, I-37134 Verona, Italy

Enzo Cazzanelli
Dipartimento di Fisica and Consorzio Nazionale Italiano di Struttura della Materia, Università degli Studi della Calabria, Ponte Bucci, Cubo 31C, I-87036 Arcavacata di Rende (CS), Italy

Adolfo Speghini
Dipartimento di Biotecnologie and Consorzio Interuniversitario per la Scienza e Tecnologia dei Materiali, Università degli Studi di Verona, Strada Le Grazie 15, I-37134, Verona, Italy

(Received 8 August 2012; revised manuscript received 26 October 2012; published 21 December 2012)

The vibrational properties of yttrium orthovanadate (YVO_4) single crystals, with tetragonal zircon structure, have been investigated by means of polarized micro-Raman spectroscopy and *ab initio* calculations. Raman spectra were taken at different polarizations and orientations carefully set by the use of a micromanipulator, so that all of the twelve Raman-active modes, expected on the basis of the group theory, were selected in turn and definitively assigned in wave number and symmetry. In particular the $E_g(4)$ mode, assigned incorrectly in previous literature, has been observed at 387 cm^{-1}. Moreover, the very weak $E_g(1)$ mode, peaked at about 137 cm^{-1}, was clearly observed only under some excitation wavelengths, and its peculiar Raman excitation profile was measured within a wide region of the visible. Finally, *ab initio* calculations based on density-functional theory have been performed in order to determine both Raman and infrared vibrational modes and to corroborate the experimental results. The rather good agreement between computational and experimental frequencies is slightly better than in previous computational works and supports our experimental symmetry assignments.

DOI: 10.1103/PhysRevB.86.214305 PACS number(s): 78.30.−j

I. INTRODUCTION

Yttrium orthovanadate (YVO_4) is one of the most important laser-host materials. In fact, when doped with rare earth (RE) ions, such as Nd^{3+}, etc., it exhibits high optical absorption coefficient, large emission cross section, and long fluorescence lifetime.[1,2] RE-doped YVO_4 single crystals are employed in highly efficient diode-pumped solid-state lasers operating in the mid-IR.[3–6] On the other hand, RE-doped YVO_4 powders provide a class of efficient nanocrystalline phosphors.[7–9] Due to its large birefringence and very wide transparency from the visible to the infrared spectral region, YVO_4 in crystal form is an excellent synthetic substitute for calcite ($CaCO_3$) and can provide crystalline polarizers for the mid-IR (as Wollaston, Rochon, and Glan prisms), besides being widely used for fiber-optic and medical applications.[10–14] Moreover, with respect to other birefringent crystals, YVO_4 has larger hardness, better water insolubility, and it is easier to fabricate large crystals of excellent optical quality at lower cost.[15–17]

The first Raman and infrared study of the vibrational spectrum of crystalline yttrium orthovanadate (YVO_4) was done by Miller *et al.*,[18] who observed nine of the twelve predicted Raman-active modes and six of the seven predicted infrared-active modes. Beside the group theoretical analysis of the lattice dynamics of YVO_4, symmetry assignments of all the observed Raman modes were attempted by Miller *et al.*,[18] in spite of the not pure polarization character of their experimental spectra. Soon after, Chaves and Porto[19] showed that the almost complete breakdown of group theoretical polarizability selection rules in YVO_4, explained by Miller *et al.*[18] in terms of the sample misalignment, was really due to strong birefringence effects in this crystal. In fact, by minimizing the birefringence effects they were able to observe some of the Raman modes missed by Miller *et al.*,[18] but, unfortunately, they failed to detect two E_g phonons among the five predicted by the group theory.[20] In the following years a series of independent Raman studies were carried out on some rare-earth vanadates, isomorphs to YVO_4, which were also unsuccessful in detecting two of the five expected E_g modes, and sometimes even other modes were missing too, as reported by Santos *et al.*[21] and references therein.

Some years ago, Bi and coworkers[22] measured the infrared reflectivity spectra on the (001) plane of YVO_4 single crystal, obtaining the frequency of all the expected IR-active modes with E_u symmetry. More recently, through a Raman spectroscopic study of the structural disorder in some crystals with zircon or scheelite structure, Voron'ko *et al.*[23] reported all the predicted bands of YVO_4 Raman spectrum, by quoting even the two missing E_g bands at 137 cm^{-1} [e.g., the E_g(V) mode according to Ref. 20] and at 444 cm^{-1} [e.g., the E_g(IV) mode of Ref. 20], respectively, both characterized by an extremely low intensity. In fact, as far as the experimental spectrum displayed in Fig. 3(a) of Ref. 23 is concerned, the E_g(V) mode of YVO_4 turns out clearly contrasted, in spite of its very

low intensity, while no spectral evidence of the claimed E_g(IV) mode, quoted at 444 cm^{-1} in the reported table of vibrational frequencies, is really provided.

Recently, pressure-dependent Raman measurements were made by Manjón *et al.*,[24] but still nine Raman-active modes were observed instead of the twelve predicted by the group theory.[20] Likewise, in a very recent Raman report on $LuVO_4$, Xu *et al.*[25] also quote nine Raman-active modes, and, in the aim to account for their deficient Raman observations, they speculate about the accidental degeneracy between of Raman modes with different symmetry.

The state of the art on YVO_4, and on rare-earth vanadates with zircon structure, consists of a series of Raman reports where nine (or ten) of the twelve expected Raman modes were properly detected either in symmetry or in wave number, besides the Voron'ko *et al.*[23] paper which claims for the identification of the whole set of twelve Raman modes of YVO_4, including the dubious one at 444 cm^{-1}.

In the present work, we report on the results of a thorough vibrational dynamics study of YVO_4 single crystal, consisting of highly symmetry-selective polarized Raman scattering measurements and of *ab initio* calculations. In fact, by adopting an innovative microsampling approach, which exploits a homemade micromanipulator to hold the sample, and by properly combining different crystal orientations and polarization settings of both incident and scattered radiation, all the twelve Raman-active modes of YVO_4 have been selectively detected and the corresponding symmetries and frequencies definitely determined. Furthermore, *ab initio* calculations based on density functional theory within the generalized gradient approximation have been performed in order to determine both the Raman and infrared vibrational frequencies. Our calculated frequencies are in slightly better agreement with experimental frequencies than previous theoretical works and definitively support our experimental symmetry assignments.

II. EXPERIMENTAL DETAILS

Single crystals of YVO_4 were obtained by a "flux growth" technique using $Pb_2V_2O_7$ as solvent. Details about the crystal synthesis and structure are reported elsewhere.[26] The as-grown crystals usually have a barlike shape with the long dimension corresponding to the c direction and the large faces corresponding to the (100) and (010) planes. The typical dimensions of the sample ranged between some hundredths on microns and about 1 mm along the basal plane, while their length varied between 2 mm and about 5 mm. The volume of the sample used for the Raman measurements was approximately $0.5 \times 0.8 \times 2.5$ mm^3.

Room-temperature polarized Raman spectra were carried out in the usual backscattering geometry from a high optical quality single microcrystal, by means of a microprobe setup provided by an Olympus microscope BX41 coupled to a triple-monochromator (Horiba-Jobin Yvon, model T64000), equipped with holographic gratings, having 1800 lines/mm, and set in double-subtractive/single configuration. The spectra were excited by the 514.5 nm line of a mixed Ar-Kr ion gas laser. At the occurrence, laser lines of different wavelength, namely the 454.5 nm, 472.7 nm, 488.0 nm, 496.5 nm, 530.9 nm, 568.2 nm, and 632.8 nm ones, were used in turn to excite the spectra. The laser beam was focused onto a spot of 5 μm in size through the lens of a 10× microscope objective with low numerical aperture (N.A. = 0.25) and the power on the sample surface was kept well below 10 mW.

Proper orientation of the single microcrystal was achieved using a homemade micromanipulator operated under direct optical inspection of a color camera interfaced to a microscope objective, the same used to focus the laser beam onto the sample. The core of the micromanipulator was a high angular-resolution goniometer which allowed for micrometric rotations of the crystal around its crystallographic c axis. The advantages provided by our innovative approach exploiting the micromanipulator to properly orient single-crystal sample with small size were elucidated and discussed in recent papers on anatase TiO_2[27] and on both xenotime YPO_4 and pretulite $ScPO_4$.[28]

According to the Damen's notation,[29] we have indicated the scattering configuration as $\bar{k}_i(\bar{E}_i, \bar{E}_s)\bar{k}_s$, where $\bar{k}_i$ and $\bar{k}_s$ are the propagation directions while $\bar{E}_i$ and $\bar{E}_s$ are the polarization directions of the incident and scattered light, respectively. In order to have the same laser power at the sample surface, all spectra were excited without modifying the polarization direction of the incident laser radiation, and the actual polarization setting, either parallel or perpendicular, was defined by the scattered radiation analyzer, coupled to a scrambler placed at the spectrometer entrance.

The scattered radiation, filtered by the fore double-monochromator, was detected at the spectrograph output by a charge coupled device (CCD) detector, with 1024×256 pixels, cooled by liquid nitrogen. Under excitation at 514.5 nm, the spectral resolution was better than 0.6 cm^{-1}/pixel, while an accurate wave number calibration of the spectrometer was achieved based on the emission lines of a Ne spectral lamp. Repeated micro-Raman measurements were run under the same experimental conditions by moving the laser spot over the exposed sample surface, and the spectra showed a very good reproducibility. No appreciable Raman scattering from possible impurities was observed. The recorded spectra were processed to remove artifact due to cosmic rays, while the luminescence background, consisting of a flat and structureless profile of very weak intensity underlying the overall Raman spectrum, was removed before the analysis of the spectra obtained under different excitation wavelengths. The Raman peaks, observed in the different scattering configurations, were fitted by Lorentzian line shapes, using a commercial fitting program.

III. POLARIZED RAMAN SPECTRA

Yttrium orthovanadate (YVO_4) possesses uniaxial crystalline structure and crystallizes in the zircon-type structure, with four formula units per unit cell, and belongs to space group D_{4h}^{19} (I41/amd), number 141 in the standard listing. A primitive cell can be chosen with two formula units (i.e., 12 atoms). A pictorial representation of this structure is given in Fig. 1: the c axis is vertical, a and b axes define the basal plane, while grid, small-gray, and large-open circles denote V, O, and Y atoms, respectively.

Several authors have reported a detailed group-theoretical analysis of phonons in the zircon-type structure, with

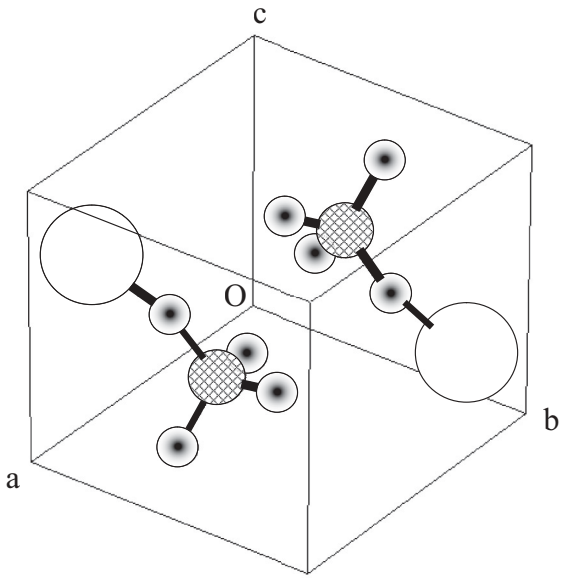

FIG. 1. Crystallographic tetragonal zircon structure of YVO_4. The c axis is vertical, a and b axes define the basal plane, while grid, small-gray, and large-open circles denote V, O, and Y atoms, respectively.

specific concern for rare-earth orthovanadate (RVO_4) compounds.[18,20,25,30] The 12 atoms of the primitive cell gives rise at the center of the Brillouin zone to 36 phonon branches of which twelve modes (i.e., the $2A_{1g}$, $4B_{1g}$, B_{2g}, and $5E_g$) are Raman active and seven modes (i.e., the $3A_{2u}$ and $4E_u$) are IR active. Following Miller *et al.*,[18] it is convenient, though in some way not fully correct, to divide both the Raman and IR active modes of orthovanadates into internal and external modes. Among the twelve Raman active modes, seven (i.e., $2A_{1g} + 2B_{1g} + 1B_{2g} + 2E_g$) are labeled as internal modes,[20,30] since, in the case of RVO_4 compounds, they originate from the crystal field splitting of the vibrational modes of oxygen atoms within the $(VO_4)^{3-}$ tetrahedral groups, four ($2B_{1g} + 2E_g$) are referred as external modes due to translations of the $(VO_4)^{3-}$ and R^{3+} ions, and one (E_g) is the librational mode of whole $(VO_4)^{3-}$ tetrahedra. The scattering tensors α, each one corresponding to a specific irreducible representation, can be written for all the Raman-active vibrational modes, i.e.,[19,30]

$$\alpha(A_{1g}) = \begin{pmatrix} a & 0 & 0 \\ 0 & a & 0 \\ 0 & 0 & b \end{pmatrix} \quad (1)$$

$$\alpha(B_{1g}) = \begin{pmatrix} c & 0 & 0 \\ 0 & -c & 0 \\ 0 & 0 & 0 \end{pmatrix} \quad (2)$$

$$\alpha(B_{2g}) = \begin{pmatrix} 0 & d & 0 \\ d & 0 & 0 \\ 0 & 0 & 0 \end{pmatrix} \quad (3)$$

$$\alpha(E_g) = \begin{pmatrix} 0 & 0 & e \\ 0 & 0 & e \\ e & e & 0 \end{pmatrix}. \quad (4)$$

These tensors are necessary to understand the polarized Raman spectra of YVO_4; in particular to study the angular dependence of the scattering intensities within the intrinsic coordinate system, based on the a,b,c crystal axes, hereafter indicated as x,y,z axes, respectively. To analyze a given tensor component α_{ij}, the scattering experiment should be arranged so that the incident light is polarized along the i direction and only the scattered light along the j direction is detected. The direction of c axis (z direction) can be found optically or by means of x-ray diffraction. In the present case the high quality of the crystals allowed for an easy optical determination of that axis. In contrast, the optical approach did not allow for the determination of the a and b axes (the basal x-y plane), and, consequently, an improper orientation of the crystal sample complicated the interpretation of the polarized spectra, in particular of those obtained in backscattering geometry. In our case, once determined the c axis, the proper orientation of the single crystal in the basal x-y plane, was achieved by means of the micromanipulator operated under direct optical monitoring.

In a crystal with D_{4h}^{19} space group such as YVO_4, a mismatch of the light polarization direction in the x-y basal plane prevents the discrimination between spectra of pure symmetries A_{1g}, B_{1g}, and B_{2g}, generating ambiguity in the phonon symmetry assignment. In fact, to select the A_{1g}, B_{1g}, and B_{2g} modes an accurate control is required on the angle between the incident and scattered polarizations and the crystal axes a and b in order to minimize the spillover effects.

Conscious of this bottleneck, we have carried out accurate Raman measurements under different polarization settings and crystal orientations so that all the independent components of the Raman polarizability tensor were explored. All polarized spectra reported hereafter were carried out in backscattering geometry with the incident radiation polarized either perpendicular to the basal x-y plane of the YVO_4 crystal or parallel to it, these two configurations being obtained by properly orientating the single crystal under the microprobing head.

Micro-Raman spectra plotted in Figs. 2(a) and 2(b), were carried out on the crystal having its crystallographic c axis perfectly aligned along the direction of the electric field of incident radiation, the scattered radiation being analyzed in parallel [as sketched inside Fig. 2(a)] or crossed [see sketch inside the Fig. 2(b)] polarization, respectively. They show, in turn, the Raman tensor components α_{zz} [Fig. 2(a)] and the α_{zx} [Fig. 2(b)] components, related to A_{1g} and E_g modes, [*here z,x indicate a set of two orthogonal directions: z is parallel to the crystallographic c axis while x belongs to basal (a-b) plane]. The above polarized Raman spectra correspond to the symmetries A_{1g} and E_g, respectively, when the basal x-y crystal plane matches the scattering plane Y-Z in the laboratory frame (L system). In particular, Fig. 2(a) displays the A_{1g} spectrum associated with the Raman tensor component α_{zz} [see Eq. (1)]. The polarizations of both the incident light and the analyzed scattered light are oriented along the crystal c axis, which corresponds to the laboratory X axis [see the sketch in Fig. 2(a)]. In this spectrum are clearly observed two well-shaped peaks centered at 379 cm^{-1} and 891 cm^{-1}. The peak at about 379 cm^{-1} presents a small but noticeable asymmetry, in the form of long tail extending on the side of the higher wave numbers.

By keeping the same crystal orientation and changing the direction of the polarization analyzer, along the Y axis of

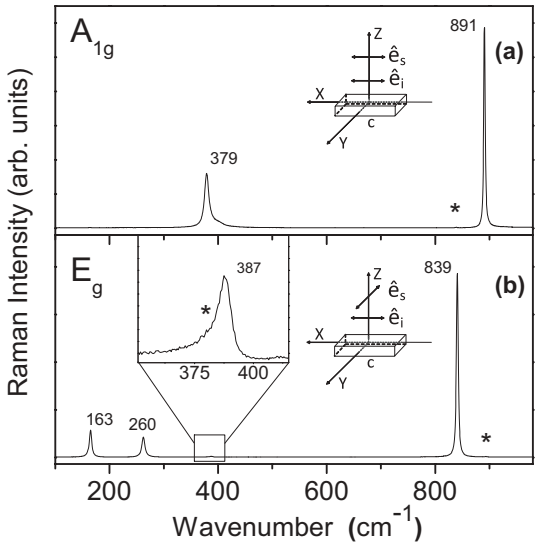

FIG. 2. As recorded micro-Raman spectra of YVO_4 carried out in backscattering geometry (with $Z' = \bar{Z}$) under excitation at 514.5 nm, for parallel (a) and crossed (b) polarization. The crystal orientation was common to both the polarization settings, as sketched in the two panels. The two panels show the spectra of symmetry A_{1g} (a) and E_g (b), respectively. The E_g mode peaked at 387 cm^{-1} can be clearly observed only after proper magnification, as evidenced in the inset of panel (b). The stars (*) label the spill of the forbidden modes.

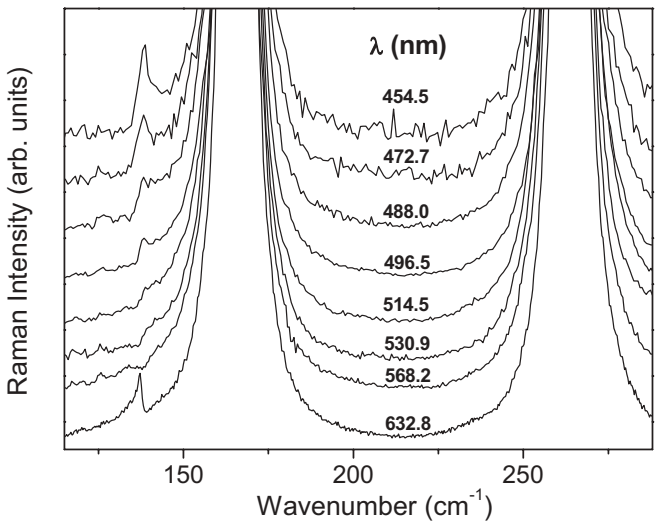

FIG. 3. Low-frequency micro-Raman spectra of YVO_4 carried out in backscattering geometry under different excitation wave lengths in crossed polarization and crystal orientation as sketched in Fig. 2(b). Each spectrum is plotted in its relative intensity scale, after normalization to amplitude of the strongest E_g mode peaked at 260 cm^{-1}. The spectra are serially displaced along the intensity axis in order to make easier the observation of the spectral evolution. The weak peak at about 137 cm^{-1}, observed only under excitation of blue and red lines, thus missing in the spectrum of Fig. 2(b), is identified as the fifth E_g mode predicted by the group theory.

Laboratory system, so that it became coplanar to the basal x-y plane of the crystal, the E_g spectrum can be selected [see Fig. 2(b)]. In fact, it is associated to the α_{zx} and α_{zy} tensor elements (or to a linear combination of them). On the basis of group theory considerations, five different modes of E_g symmetry are expected to be observed. Now the spectrum plotted in Fig. 2(b) clearly shows three modes E_g peaked at 163 cm^{-1}, 260 cm^{-1}, and 839 cm^{-1}, respectively, all of them being clearly contrasted, showing a noticeable intensity, although unlike. By the way, a finer inspection of the spectral region close to 400 cm^{-1}, reveals the presence of an additional, hardly appreciable peak of E_g symmetry. Its intensity is so small that a proper magnification of the Raman signal recorded in this region was necessary in order to make it easily observable [see the inset of Fig. 2(b)]. This one clearly shows the E_g mode peaked at 387 cm^{-1}, together with a hardly appreciable tail on its low-frequency side due to the leakage of the A_{1g} mode at 379 cm^{-1}, there labeled by a star (*).

This E_g mode should correspond to the E_g(IV) predicted by Elliott *et al.*,[20] who were not able to observe it even at low temperatures.[20] Our finding, then, clearly contradicts the reported attribution of the faint spectral feature observed by Voron'ko *et al.*[23] at 444 cm^{-1} to the E_g(IV) mode. However, in spite of the inconsistency of their claimed observation of the E_g(IV) mode, these authors were able to identify the missing fifth E_g(V) mode peaked at about 137 cm^{-1} in the Raman spectrum of YVO_4 excited at 488.0 nm. Stimulated by the Voron'ko *et al.*[23] observation, we decided to explore the low-frequency spectrum by using different excitation lines, in addition to the 514.5 nm so far used by us. The E_g-symmetry micro-Raman spectra of YVO_4 carried out in the wave-number region between 115 cm^{-1} and 290 cm^{-1} under eight different excitation wavelengths in backscattering geometry are plotted in in Fig. 3, after being normalized to the amplitude of the much stronger E_g mode peaked at 260 cm^{-1}. This figure clearly confirms the presence of the further E_g mode at about 137 cm^{-1} (i.e., the missing fifth E_g mode) according to the group theoretical predictions. Moreover a peculiar dependence of the intensity on the excitation wavelength is observed. This mode is not observable, even keeping comparable experimental conditions for the power excitation, in the green-yellow region of the visible, while it can be observed under red excitation and even more efficiently for excitation in the blue-violet region. This behavior could explain the lack of observations generally resulting from the literature.

In conclusion, the E_g-symmetry Raman spectrum of YVO_4 definitely consists of five different modes, in full agreement with the group theory predictions. They are peaked at about at 137 cm^{-1}, 163 cm^{-1}, 260 cm^{-1}, 387 cm^{-1}, and 839 cm^{-1}, respectively, and are numbered in Table I according to the increasing energy, this list having a different order from that proposed by Elliot *et al.*[20]

Finally, regardless to their intensity, our α_{zx} polarized Raman spectrum, as well as the α_{zz} one, suggests that a nearly perfect alignment of the electric field vector of the incident light along the c axis of the inspected crystal was achieved during the measurements. In fact, no appreciable leakage of forbidden modes is displayed by α_{zz} spectrum, while it is slightly more evident in α_{zx} spectrum, but without any effect on the symmetry assignments above carried out.

We turn now to consider the polarized spectra carried out in backscattering geometry from the crystal oriented in such a way that its c axis resulted parallel to the propagation

TABLE I. Observed and calculated optical frequencies of YVO_4 (in cm^{-1}) at the Γ point. Columna (a) refer to the present work, column (b) to Ref. 23, column (c) to Ref. 20, columns (d) to Ref. 24, columns (e) to Ref. 18, columns (f) to Ref. 44, and column (g) to Ref. 22. The two indices $|\overline{\Delta}|$ and $\overline{|\Delta_r|}\%$ (see text), listed at the end of table, are calculated (i) for all the 19 vibrational modes (Raman + IR), and (ii) for the Raman active modes only.

Raman modes	Exp.(a)	Exp.(b)	Exp.(c)	Exp.(d)	Exp.(e)	Th.(a)	Th.(f)	Th.(d)	Th.(d)
$E_g(1)$	137	137	–	–	–	142	136	134	131
$B_{1g}(1)$	157	157	156	157	157	166	164	163	150
$E_g(2)$	163	163	164	163	162	171	168	168	157
$E_g(3)$	260	260	260	260	260	249	282	276	238
B_{2g}	260	260	260	260	260	269	256	256	255
$B_{1g}(2)$	267	267	265	–	–	252	275	274	252
$A_{1g}(1)$	379	378	379	378	379	374	383	380	360
$E_g(4)$	387	444[a]	–	–	–	409	379	376	371
$B_{1g}(3)$	490	490	490	489	489	478	487	480	461
$B_{1g}(4)$	816	817	817	816	817	824	865	862	811
$E_g(5)$	839	840	839	839	840	828	876	874	825
$A_{1g}(2)$	891	891	891	891	891	902	931	924	875
Infrared modes	Exp.(e)	Exp.(g)				Th.(a)	Th.(f)		
$E_u(1)$	196	193				200	199		
$E_u(2)$	261	262				251	271		
$A_{2u}(1)$	310	–				228	249		
$E_u(3)$	–	310				319	310		
$A_{2u}(2)$	455	–				433	456		
$E_u(4)$	778	778				778	825		
$A_{2u}(3)$	803	–				815	856		
Raman + IR modes									
$\overline{\lvert\Delta\rvert}$						14.0	19.2	–	–
$\overline{\lvert\Delta_r\rvert}\%$						4.4%	4.1%	–	–
Raman modes									
$\overline{\lvert\Delta\rvert}$						10.4	15.7	14.7	13.3
$\overline{\lvert\Delta_r\rvert}\%$						3.3%	3.3%	3.2%	3.9%

[a]In Ref. 23 the $E_g(4)$ mode was erroneously assigned at 444 cm^{-1} (see text).

direction of the laser beam, so that the electric field of the incident radiation belongs to basal plane x-y of the YVO_4 crystal. In fact, when this particular configuration is matched, the electric field of the backscattered radiation also belongs to the basal plane x-y. In our case, once we determined the c axis, the proper orientation of the single crystal in the basal x-y plane was achieved by means of the micromanipulator operated under direct optical monitoring. This step was crucial in view of the selectively excited Raman modes associated to polarizability tensor components belonging to the basal plane x-y of the YVO_4 crystal, which, according to Eqs. (1)–(3), can have symmetry A_{1g}, B_{1g}, or B_{2g}. Moreover, in order to fully resolve and discriminate these modes, it is necessary to accurately control the polarization direction of both the incident and scattered radiation with respect to the crystallographic axis a (or b).

In this specific case a good correspondence between the light polarization direction and the true crystal axes was found by rotating step by step the crystal around its c axis, which was previously aligned along the propagation direction of incident and scattered light, labeled Z in the laboratory frame. In fact, the relations between the Raman tensor elements written in the laboratory frame and the ones of the crystal frame, with the Z axis corresponding to the crystal c axis, and X, Y generic orthogonal directions belonging to the a-b basal plane, can be expressed as function of the angle θ of rotation around the c axis (Z in laboratory frame), in the following way:

$$\alpha_{XX} = (\cos^2\theta)\alpha_{xx} + (\sin^2\theta)\alpha_{yy} + (2\sin\theta\cos\theta)\alpha_{xy} \quad (5)$$

and

$$\alpha_{XY} = (\sin\theta\cos\theta)\alpha_{xx} - (\cos\theta\sin\theta)\alpha_{yy} + (\sin^2\theta - \cos^2\theta)\alpha_{xy}, \quad (6)$$

where the assumption $\alpha_{xy} = \alpha_{yx}$ was also made, derived from the symmetry of Raman tensor. As a consequence of Eqs. (5) and (6) the A_{1g} spectrum, observed in the adopted backscattering setting, is expected to maintain the same intensity, independently from the value of angle θ, when the XX (parallel) polarization combination is observed, while its intensity results always zero for XY (crossed) polarization, at any value of θ. On the contrary, either for parallel polarizations XX or for crossed polarizations XY, the intensities of B_{1g} and B_{2g} modes exhibit strong oscillations vs θ, in the opposite way, between a maximum and a near-zero value, when the rotation angle varies of 45°. Thus, in order to rule out the occurrence of the A_{1g} modes in the observed spectra, it was mandatory to run the measurements in crossed polarization. The complementary behavior of Raman intensity for B_{1g} and B_{2g} modes in this particular setting can be understood if we

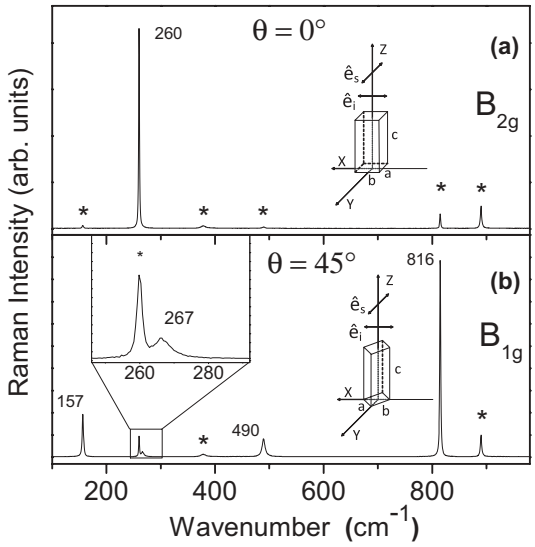

FIG. 4. As-recorded micro-Raman spectra of YVO_4 carried out in backscattering geometry (with $Z' = \bar{Z}$) under excitation at 514.5 nm, in crossed polarization for the two different crystal orientations sketched in the two panels (see, also, text for more details). The two panels show the spectra of symmetry B_{2g} (a) and B_{1g} (b), respectively. The B_{1g} mode peaked at 267 cm^{-1} turns out much easily observable after proper magnification, as evidenced in the inset of (b). Finally, the stars (*) label the spill of the forbidden modes. Note that the spilling intensity of the A_{1g} modes is independent of the crystal orientation.

consider the particular form of the tensor elements for the Raman active modes belonging to these two symmetries in the tetragonal orthovanadates with zircon-type structure. In fact, from Eqs. (2) and (3) we obtain, respectively

$$\alpha_{XY}(B_{1g}) = \sin(2\theta)\alpha_{xx} \tag{7}$$

$$\alpha_{XY}(B_{2g}) = -\cos(2\theta)\alpha_{xy}. \tag{8}$$

The experimental Raman spectra recorded in crossed (XY) polarization in correspondence to two values of the rotation angle θ differing by 45°, which alternatively display the B_{2g} spectrum or the B_{1g} one, are plotted in Figs. 4(a) and 4(b), respectively, where only a minor presence of the A_{1g} modes, due to spillover effects, can be observed, too. The B_{2g} spectrum, associated to the intrinsic α_{xy} or α_{yx} component of the Raman tensor, was observed in crossed (XY) polarization for the value of $\theta = 0°$, for which the spectral intensity of the B_{1g} modes approached its minimum value. In agreement with the group theory predictions, in this spectrum only the B_{2g} mode can be observed, and it appears as a very sharp, symmetric peak centered at about 260 cm^{-1} [see Fig. 4(a)].

Alternatively, in the aim to isolate the B_{1g} spectrum, the measurement was carried out in the backscattering geometry in crossed (XY) polarization for the value of θ giving rise to the maximum intensity quenching of the B_{2g} mode (i.e., $\theta = 45°$). The experimental spectrum measured in this scattering conditions is plotted in Fig. 4(b): four distinct Raman modes of B_{1g} symmetry are clearly observed at 157 cm^{-1}, 267 cm^{-1}, 490 cm^{-1}, and 816 cm^{-1}, respectively. All these modes are clearly visible in the as-recorded spectrum, despite of their remarkably different relative intensities as well as of the presence of spilling modes of forbidden symmetry. In fact, due to the extremely low intensity of one of them (i.e., the one peaked at about 267 cm^{-1}) it was mandatory to properly magnify the spectral intensity in the region of the peak occurrence in order to observe it [see inset of Fig. 4(b)].

IV. *AB INITIO* CALCULATIONS

The Raman and infrared vibrational frequencies of YVO_4 crystal have been also computed by using *ab initio* calculations based on a density functional theory in the generalized gradient approximation. In this computational study the CRYSTAL06 program[31] was adopted. It is a periodic *ab initio* program, which uses a Gaussian-type basis set to represent the crystalline orbitals. Further details on basis sets and computational parameters, as well as input and output files, can be found at the CRYSTAL website.[32] In this specific case all-electron basis sets have been used with 86-411d4G contractions (one *s*, four *sp,* and one *d* shell) for vanadium atoms,[33] 8-411(one *s* and three *sp* shells) for oxygen atoms,[34,35] 9766-31d31 (one *s*, two *sp*, one *d*, two *sp*, and two *d* shells) for yttrium.[36]

Pure density-functional theory calculations have been made by using Perdew-Becke-Ernzerhof exchange and correlation functional.[37] Exchange-correlation functionals of other kinds have been also tested, but the results were worse. The accuracy level in evaluating Coulomb and exchange series is controlled by five parameters, for which standard values have been used (6 6 6 6 12). To ensure a good convergence, self-consistent field convergence thresholds of 10^{-7} Hartree have been adopted for both eigenvalues and total energies. A Monkhorst-Pack shrinking factor[38,39] equal to 8 is used to compute the integration on the Brillouin zone. Vibrational frequencies have been calculated within the harmonic approximation. The frequencies have been obtained, at the Γ point, by diagonalizing the mass-weighted Hessian matrix, whose (i, j) element is defined as $W_{ij} = H_{ij}/\sqrt{M_i M_j}$, M_i and M_j being the masses of the atoms associated with i and j coordinates, respectively. A more complete description of the method and other details on computational aspects can be found in Refs. 40 and 41.

In YVO_4 crystal, the geometry optimization gives the cell parameters $a = b = 7.1973$ Å, $c = 6.4214$ Å and $a/c = 1.121$, which differ from the experimental values[42,43] by about 1.1, 2.1, and 1.0%, respectively. These values for the cell parameters have been used in the frequencies calculation reported below. Table I displays the calculated frequencies of the optical modes (Raman and infrared) of YVO_4 compared with the available experimental data, including the new Raman measurements performed in the present work.

The calculated frequencies (ν^{cal}) have been compared with the experimental frequencies (ν^{exp}) through *i*) the average of the absolute difference *ii*) the average of the absolute relative difference (in percentage), respectively defined in the following

$$\overline{|\Delta|} = \frac{1}{N}\sum_{i=1}^{N}\left|\nu_i^{cal} - \nu_i^{exp}\right| \tag{9}$$

and

$$\overline{|\Delta_r|}\% = \frac{100}{N}\sum_{i=1}^{N}\left|\frac{\nu_i^{\mathrm{cal}} - \nu_i^{\mathrm{exp}}}{\nu_i^{\mathrm{exp}}}\right|,$$

where the index $i = 1, \ldots, N$ runs over the 19 optical modes listed in Table I. We have considered as experimental frequencies ν_i^{exp} the average of the available experimental data [i.e., the average of columns (a), (b), (c), (d), and (e) of Table I] for the Raman modes (without considering the $E_g(4)$ mode of column (b), columns (e), and column (g) for the infrared modes. The two indices are reported at the end of Table I. For comparison, also the indices related to the frequencies calculated by Vali, Manjón, and coworkers are reported.[24,44] The comparison between theory and experiment has been made (i) for all the 19 optical modes; (ii) for the Raman modes only, in order to have a comparison with the computational works performed by Manjón *et al.*,[24] who calculated only the frequencies of the Raman modes. The two indices show a very good agreement between our calculations and experimental data, overall slightly better than that achieved previously. Moreover, the present computational results corroborate our symmetry assignment of the $E_g(1)$ and $E_g(4)$ Raman modes.

V. DISCUSSION

The above-reported results of polarized Raman scattering experiments carried out from an oriented YVO_4 crystal and of *ab initio* calculations of the vibrational frequencies of this crystal give a detailed and definitive description of the vibrational dynamics of this compound.

In fact, a thorough description of the vibrational dynamics of the prototype compound of orthovanadate family with zircon-type structure is provided in our present work, by showing reliable experimental evidences of some Raman modes, which were either not reported in the existing literature[18–21] or wrongly assigned in wave number.[23] In particular, the difficult detection of the systematically missing $E_g(4)$ mode, which is characterized by an extremely weak intensity, fully confirms the correctness of the hypothesis formulated by Elliott *et al.*[20] On the other hand, what is also more important, by comparison with the compounds of the orthophosphate family[28,45,46] and rare-earth arsenates[47] with the same zircon-type structure, we can infer that, as far as the other compounds of this orthovanadate family are considered, the frequency of this E_g mode should be nearly independent of the rare-earth ion mass, and, therefore, that it should occurs close nearby at the same frequency as it is observed in YVO_4. Moreover, the highly symmetry-selective measurements of this study point out the added value of our experimental approach based on the use of a micromanipulator to properly orientate the sample. Our experimental results are in agreement, for most of the issues, with the existing literature.

However, some particular achievements deserve supplementary comments and a more detailed comparison with previous findings, in some cases partial or contradictory. The complete and unambiguous detection of all the predicted five E_g modes, can be considered one of the most important achievements in the present work. In fact, the group theoretical predictions of five E_g modes can be fully satisfied if an adequate integration time of measurement is adopted, so that it allows for a clear detection of the 387 cm^{-1} and the 137 cm^{-1} modes, much weaker than the other modes of the same symmetry. The weakness of these two E_g modes [i.e., the E_g(IV) and the E_g(V)] according to Elliott *et al.*,[20] cannot be explained on the basis of experimental considerations, but it might be surely invoked to justify the fact that neither of these modes was observed in the pioneering Raman investigations by Miller *et al.*[18] and by Chaves and Porto[19] on YVO_4 single crystals, nor in a more recent study on rare-earth orthovanadates by Santos *et al.*[21] and references therein.

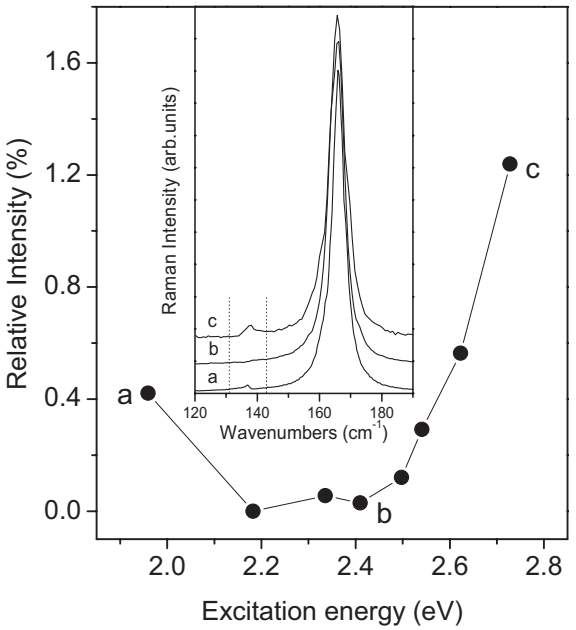

FIG. 5. Raman excitation profile of the weak E_g mode peak at about 137 cm^{-1}. The relative intensity of this peak was obtained by integrating the area in the spectral region limited by the two dotted vertical lines, after the subtraction of interpolated spectral profile saddling the peak outside this region, and then normalizing it to the intensity of the E_g mode peak at about 163 cm^{-1}. The inset show the partial spectra corresponding to the values a, b, and c of the excitation profile. The line connecting the dots is the guide for the eye.

Furthermore, the E_g(V) mode becomes practically undetectable even in these measurement conditions if the wrong excitation wavelength is chosen. The extensive investigation on the spectral shape dependence on excitation wavelength, reported in Fig. 3, allows us to definitely explain the apparent contradictions between the results of different works on the subject. As well evident from Fig. 3, the yellow-green region of the spectrum, much exploited in Raman measurements, corresponds to a substantial quenching of the 137 cm^{-1} mode intensity, which inhibits the discrimination of this mode from the tail of the much stronger 163 cm^{-1} one. An even stronger evidence of the E_g(V) mode antiresonant behavior is provided by the plot of its properly normalized intensity vs excitation energy, which is shown in Fig. 5. The intensity of the 137 cm^{-1} mode, calculated after deconvolution from the stronger 163 cm^{-1} mode, was normalized to the intensity of this last one, but the resulting behavior of the Raman excitation profile was practically the same after normalization to that of the 260 cm^{-1} E_g mode. Several theoretical models[48]

can be used to explain such antiresonance behavior, all of them deriving from coupling between vibrational mode and electronic transitions of the system. Unfortunately the small size of our crystal did not allow us to carry out any reliable optical absorption spectrum on it, and therefore to proceed with the optical detection of the possible electronic transition involved in the phenomenon. However, it can be of some interest to point out a difference in the asymmetric line shape of the E_g(V) mode for excitation energies above and below the intensity quenching region (see Fig. 3): for red excitation (632.8 nm) the long tail of the mode is on the lower-frequency side, and the sharp drop on the high-frequency side, while for excitation by blue lines, when the mode is well detected, the reverse situation occurs. This fact could suggest to address toward a Fano formalism[49,50] for a more exhaustive theoretical explanation of the observed phenomenology.

VI. CONCLUSION

In this work, the vibrational properties of yttrium orthovanadate (YVO_4) have been investigated by means of both polarized Raman spectroscopy and *ab initio* calculations. Symmetry-selective measurements have been carried out using a micromanipulator to finely orient the crystal. Through a proper polarization analysis, all the 12 Raman-active modes of YVO_4 have been contrasted in turn and definitively assigned in symmetry. In particular, the $E_g(1)$ and $E_g(4)$ vibrational modes, corresponding to E_g(V) and E_g(IV) modes quoted by Elliott *et al.*,[20] have been detected at 137 cm^{-1} and 387 cm^{-1}, respectively, and a peculiar antiresonant dependence on excitation wavelength has been measured for the lowest-frequency one. Finally, *ab initio* calculations based on density-functional theory have been performed to calculate the Raman and infrared vibrational modes. The agreement between computational and experimental frequencies is very good, better than the one achieved in previous computational works.

ACKNOWLEDGMENTS

The authors are grateful to Professor M. Bettinelli for providing them with the samples. One of the authors (B.R.) acknowledges the financial support of the Regione Veneto within the Programma Operativo FSE 2007-13. The research was partially funded by the Fondazione Cariverona through a contract with the University of Verona.

*Corresponding author: gino.mariotto@univr.it

[1] T. Jensen, V. G. Ostroumov, J. P. Meyn, G. Huber, A. I. Zagumennyi, and I. A. Shcherbakov, Appl. Phys. B: Lasers Opt. **58**, 373 (1994).
[2] C. H. Huang, G. Zhang, Y. Wei, L. X. Huang, H. Y. Zhu, and X. J. Huang, Optik **121**, 595 (2010).
[3] J. R. O. Connor, Appl. Phys. Lett. **9**, 407 (1996).
[4] J. D. Kingsley and G. W. Ludwig, J. Appl. Phys. **41**, 370 (1970).
[5] R. A. Fields, M. Birnbaum, and C. L. Fincher, Appl. Phys. Lett. **51**, 1885 (1987).
[6] A. Di Lieto, P. Minguzzi, A. Piratsu, S. Sanguinetti, and V. Magni, Appl. Phys. B **75**, 463 (2002).
[7] A. K. Levine and F. C. Palilla, Appl. Phys. Lett. **5**, 118 (1964).
[8] A. Huignard, T. Gacoin, and J. P. Boilot, Chem. Mater. **12**, 1090 (2000).
[9] M. Yu, J. Lin, Z. Wang, J. Fu, S. Wang, H. J. Zhang, and Y. C. Han, Chem. Mater. **14**, 2224 (2002).
[10] P. P. Yaney and L. G. DeShazer, J. Opt. Soc. Am. **66**, 1405 (1976).
[11] M. Bass, IEEE J. Quantum Electron. **11**, 938 (1975).
[12] C. H. Huang, J. C. Chen, and C. Hu, J. Cryst. Growth **211**, 237 (2000).
[13] W. Ryba-Romanowski, Cryst. Res. Technol. **38**, 225 (2003).
[14] K. Yonezawa, Y. Kozawa, and S. Sato, Opt. Lett. **31**, 2151 (2006).
[15] S. K. Lin, L. T. Li, and J. Z. Chen, Spectroscopy and Spectral Analysis **23**, 474 (2003).
[16] S. Wu, G. Wang, and J. Xiea, J. Cryst. Growth **266**, 496 (2004).
[17] G. Li, K. Chao, H. Peng, and K. Chen, J. Phys. Chem. C **112**, 6228 (2008).
[18] S. A. Miller, H. H. Caspers, and H. E. Rast, Phys. Rev. **168**, 964 (1968).
[19] A. Chaves and S. P. S. Porto, Solid State Commun. **10**, 1075 (1972).
[20] R. J. Elliott, R. T. Harley, W. Hayes, and S. R. P. Smith, Proc. R. Soc. London, Ser. A **328**, 217 (1972).
[21] C. C. Santos, E. N. Silva, A. P. Ayala, I. Guedes, P. S. Pizani, C. K. Loong, and L. A. Boatner, J. Appl. Phys. **101**, 053511 (2007).
[22] C. Z. Bi, J. Y. Ma, J. Yan, X. Fang, D. Z. Yao, B. R. Zhao, and X. G. Qiu, Eur. Phys. J. B **51**, 167 (2006).
[23] Yu. K. Voron'ko, A. A. Sobol, V. E. Shukshin, A. I. Zagumenny, Yu. D. Zavartsev, and S. A. Kutovo, Phys. Solid State **51**, 1886 (2009).
[24] F. J. Manjón, P. Rodríguez-Hernández, A. Muñoz, A. H. Romero, D. Errandonea, and K. Syassen, Phys. Rev. B **81**, 075202 (2010).
[25] M. Xu, H. Yu, H. Zhang, X. Xu, and J. Wang, J. Rare Earths **29**, 207 (2011).
[26] E. Cavalli, M. Bettinelli, A. Belletti, and A. Speghini, J. Alloys Compd. **341**, 107 (2002).
[27] M. Giarola, A. Sanson, F. Monti, G. Mariotto, M. Bettinelli, A. Speghini, and G. Salviulo, Phys. Rev. B **81**, 174305 (2010).
[28] M. Giarola, A. Sanson, A. Rahman, G. Mariotto, M. Bettinelli, A. Speghini, and E. Cazzanelli, Phys. Rev. B **83**, 224302 (2011).
[29] T. C. Damen, S. P. S. Porto, and B. Tell, Phys. Rev. **142**, 570 (1966).
[30] P. Dawson, M. M. Hargreave, and G. R. Wilkinson, J. Phys. C **4**, 240 (1971).
[31] R. Dovesi, V. R. Saunders, C. Roetti, R. Orlando, C. M. Zicovich-Wilson, F. Pascale, K. Doll, N. M. Harrison, B. Civalleri, I. J. Bush, P. D'Arco, and M. Llunell, *Crystal06 User's Manual* (Università di Torino, Torino, 2006).
[32] Website: [www.crystal.unito.it]
[33] W. C. Mackrodt, N. M. Harrison, V. R. Saunders, N. L. Allan, M. D. Towler, E. Apra', and R. Dovesi, Philos. Magaz. A **68**, 653 (1993).
[34] J. Muscat, N. M. Harrison, and G. Thornton, Phys. Rev. B **59**, 2320 (1999).
[35] J. Scaranto and S. Giorgianni, J. Mol. Struct. Theochem **858**, 72 (2008).

[36]M. D. Towler [www.tcm.phy.cam.ac.uk/mdt26/crystal.html] (1995).
[37]J. P. Perdew, K. Burke, and M. Ernzerhof, Phys. Rev. Lett. **77**, 3865 (1996).
[38]C. Pisani, R. Dovesi, and C. Roetti, *Hartree-Fock ab initio Treatment of Crystalline Systems*, Lecture Notes in Chemistry, Vol. 48 (Springer Verlag, Heidelberg, 1988).
[39]H. Monkhorst and J. Pack, Phys. Rev. B **13**, 5188 (1976).
[40]C. M. Zicovich-Wilson, F. Pascale, C. Roetti, V. R. Saunders, R. Orlando, and R. Dovesi, J. Comput. Chem. **25**, 1873 (2004).
[41]F. Pascale, C. M. Zicovich-Wilson, F. L. Gejo, B. Civalleri, R. Orlando, and R. Dovesi, J. Comput. Chem. **25**, 888 (2004).
[42]J. A. Baglio and G. Gashurov, Acta Crystal. B **24**, 292 (1968).
[43]B. C. Chakoumakos, M. M. Abraham, and L. A. Boatner, J. Solid State Chem. **109**, 197 (1994).
[44]R. Vali, Solid State Comm. **149**, 1637 (2009).
[45]P. C. Becker, N. Edelstein, G. M. Williams, J. J. Bucher, R. E. Russo, J. A. Koningstein, L. A. Boatner, and M. M. Abraham, Phys. Rev. B **31**, 8102 (1985).
[46]R. Mittal, S. L. Chaplot, N. Choudhury, and C. K. Loong, J. Phys.: Cond. Matter **19**, 446202 (2007).
[47]G. Barros, C. C. Santos, A. P. Ayala, I. Guedes, L. A. Boatner, and C. K. Loong, J. Raman Spectr. **41**, 694 (2010).
[48]S. Hassing, J. Raman Spectr. **28**, 739 (1997).
[49]U. Fano, Phys. Rev. **124**, 1866 (1961).
[50]D. L. Rousseau and S. P. S. Porto, Phys. Rev. Lett. **20**, 1354 (1968).